Applied Energy 102 (2013) 850–859

Contents lists available at SciVerse ScienceDirect

Applied Energy

journal homepage: www.elsevier.com/locate/apenergy

Metabolic phenotyping of the cyanobacterium *Synechocystis* 6803 engineered for production of alkanes and free fatty acids

Ping Hu [a], Sharon Borglin [a], Nina A. Kamennaya [a], Liang Chen [a,b], Hanwool Park [a], Laura Mahoney [a], Aleksandra Kijac [c], George Shan [c], Krystle L. Chavarría [a], Chunmin Zhang [a,d], Nigel W.T. Quinn [a], David Wemmer [c], Hoi-Ying Holman [a,b], Christer Jansson [a,*]

[a] *Lawrence Berkeley National Laboratory, Berkeley, CA, USA*
[b] *The Advanced Light Source (ALS), Berkeley, CA, USA*
[c] *Department of Chemistry, UC Berkeley, CA, USA*
[d] *College of Environmental Science and Engineering, Tongji University, Shanghai, China*

HIGHLIGHTS

- *Synechocystis* 6803 was engineered for enhanced photosynthetic conversion of CO_2 to alkanes.
- *Synechocystis* 6803 was engineered for accumulation of free fatty acids.
- Single-cell metabolic phenotyping was performed using SR-FTIR spectromicroscopy.
- Multivariate analysis of SR-FTIR data revealed biochemical shifts in engineered cells.
- SR-FTIR spectromicroscopy provides a high-throughput tool for screening engineered cells.

ARTICLE INFO

Article history:
Received 14 January 2011
Received in revised form 24 August 2012
Accepted 27 August 2012
Available online 8 October 2012

Keywords:
Alkanes
Cyanobacteria
Fatty acids
FTIR
Metabolic engineering
Metabolic phenotyping
Synechocystis 6803

ABSTRACT

We demonstrate a simple high-throughput single-cell approach that exploits the ultrahigh brightness and non-invasive nature of synchrotron infrared beam to characterize strains of the cyanobacterium *Synechocystis* 6803 (*S.* 6803) constructed with altered metabolic traits affecting the acyl-CoA pool. Their metabolic responses to the modified traits were phenotyped by single-cell synchrotron radiation Fourier transform infrared (SR-FTIR) spectromicroscopy and multivariate analysis. SR-FTIR difference spectra and cluster vector plots segregated the strains as phenotypic populations based on signals in the hydrocarbon and biomolecular fingerprint regions, although each population incorporated a stochastic distribution of cells with different metabolic properties. All engineered strains exhibited an increase in FTIR features attributed to functional groups in hydrocarbon, fatty acid (FA), and/or FA ester chains, and a decrease in polysaccharide features. The metabolic signatures obtained by SR-FTIR were consistent with detailed qualitative and quantitative metabolic information provided in GC/MS/NMR data. A strain with extra copies of the *FAR* and *FAD* genes, encoding, respectively, the fatty acyl-ACP reductase and fatty aldehyde decarbonylase enzymes in the alkane biosynthesis pathway, showed up to a fivefold increase in the intracellular levels of heptadecane, a threefold increase in 9-heptadecene, and a significant increase in secreted 16:0 and 18:0 free FAs (FFAs). Inactivation of the *AAS* gene, encoding acyl-ACP synthetase, prevented re-thioesterification of FFAs generated from membrane lipid recycling and led to elevated levels and of intracellular FFAs of an altered composition, and a decrease in heptadecane and secreted FFAs. Introduction of a *FatB* gene, encoding a thioesterase (TE), which catalyzes the liberation of FFAs from acyl-ACP, yielded little effect in itself. However, the activity of the TE enzyme was clearly manifested in combination with *AAS* inactivation; A TE-containing train lacking AAS showed a dramatic (30-fold) increase in intracellular FFAs (with the majority being 16:0) and increases in heptadecane and secreted FFAs.

* Corresponding author. Tel.: +1 510 486 7541; fax: +1 510 486 7152.
E-mail address: cgjansson@lbl.gov (C. Jansson).

0306-2619/$ - see front matter © 2012 Published by Elsevier Ltd.
http://dx.doi.org/10.1016/j.apenergy.2012.08.047

1. Introduction

Cyanobacteria, like algae and plants can use solar power to capture CO_2 via the Calvin–Benson–Bassham (CBB) cycle and convert it to a suite of organic compounds.

As opposed to microalgae that can accumulate large amounts of triacylglycerols (TAGs) as storage lipids, the cyanobacteria studied to date produce little or no TAGs, but their FAs are directly shuttled to membrane lipid synthesis. Conversely, cyanobacteria, which are Gram-negative bacteria, are well suited for synthetic biology and metabolic engineering approaches aimed at redirecting carbon flux in lipid metabolism to specific biofuel molecules, including ethanol, butanol, biodiesel, and hydrocarbon biofuels. First, whereas in plants and algae, including microalgae, lipid metabolism involves several different cellular compartments, in cyanobacteria, lipid metabolism occurs via soluble or membrane-bound enzymes in the cytosol. Second, being bacteria, cyanobacteria are amenable to homologous recombination, which allows rapid site-directed mutagenesis, gene insertions, replacements, and deletions in a precise, targeted and predictable manner [1–6]. Phototrophic biosynthesis of high-density liquid biofuels in cyanobacteria could augment microbial production of biodiesel and hydrocarbons in heterotrophic bacteria such as *Escherichia coli*.

Fatty acid (FA) biosynthesis in bacteria is accomplished by a type II FA synthase (FASII), a multienzyme system utilizing a freely dissociable acyl carrier protein ACP [2,7]. The products of FASII are released as acyl-ACPs and may be directly incorporated into membrane lipids by two acyltransferases, glycerol-3-phosphate acyltransferase (GPAT; EC 2.3.1.15), and 1-Acylglycerol-3-phosphate acyltransferase (AGPAT; EC 2.3.1.51) that each attaches a FA to the glycerol 3-phosphate (G3P) backbone to form the key intermediate, phosphatidic acid (PA) [8,9]. In plants and algae, *de novo* FA synthesis occurs in the plastids, which also exhibit the FASII machinery. In the plastids, acyl-ACPs are hydrolyzed by Acyl-ACP thioesterases (TE; EC 3.1.2.14, e.g. FatB in Arabidopsis) to yield free FAs for transport across the plastid envelope. Upon arrival at the outer plastid surface, the free FAs are re-activated by Acyl-CoA synthetase (FadD; EC 6.2.1.3) to form acyl-CoA. Acyl-CoA is the starting substrate for synthesis of triacylglycerides (TAGs), but can also be used for ß-oxidation and for biosynthesis of membrane lipids. Cyanobacteria like many other bacteria lack TE enzymes that act on FA-ACPs, and formation of free FAs mainly occurs during recycling of membrane lipids or degradation of acylated proteins [10].

The fatty acyl-ACP product from FA synthesis is a crossroad metabolite for the potential photosynthetic production of lipid-based biofuels in cyanobacteria (Fig. 1). As previously demonstrated [4], by the introduction of *TE* genes acyl-ACP can be hydrolyzed to free FAs (FFAs) for downstream chemical processing to fuels. As has been shown for *E. coli* [11], the possibility also exists to convert FFAs directly to FA methylesters (FAMEs), i.e., biodiesel, *in vivo* by endowing cyanobacteria with genes for a suitable FA methyltransferase (FAMTase). Further, acyl-ACP in cyanobacteria is the substrate for alkane biosynthesis in a two-step reaction involving the enzymes fatty acyl-ACP reductase (FAR) and fatty aldehyde decarbonylase (FAD) [2,3,12] (Fig. 1).

The purpose of the work described in this paper was to demonstrate the simple single-cell synchrotron radiation SR-FTIR spectromicroscopy approach with multivariate analysis as a high-throughput diagnostic tool to study metabolic shifts in the cyanobacterium *Synechocystis* 6803 (*S.* 6803) engineered for increased accumulation of FFAs and alkanes. Because biomolecules interact non-destructively with infrared in the mid-infrared region (~2.5–12.5 μm wavelength, or ~4000–800 cm^{-1} wavenumber) [13], and because mid-infrared photons emitted from a synchrotron source can easily be focused onto a measurement area with a micrometer accuracy [14], we have developed SR-FTIR spectromicroscopy to study the chemistry changes in single or in small groups of several individual live microbial cells in real time [14,15]. To overcome the challenge of understanding a large and complex data set from the intricate biological systems, such as relating the functional metabolism features to the vibrational frequencies (wavenumbers) of the molecules, we used multivariate approaches including principal component analysis (PCA) and linear discriminant analysis (LDA). These data reduction methodologies allow identification of both biochemical distinctions and heterogeneity within cellular systems, which can then be related to discriminating vibrational frequencies in the infrared spectra [16]. The amount and detailed composition of FFAs, alkanes and other metabolites in the strains were determined by GC/MS and NMR spectroscopy, which also confirmed the validity of the SR-FTIR approach.

2. Material and methods

2.1. Chemicals and reagents

Chemicals, kits, primers, and reagents were from common commercial vendors.

2.2. Cyanobacterial strains, growth conditions, and transformation

S. 6803 was obtained from The Pasteur Culture Collection (PCC; http://www.pasteur.fr/ip/easysite/go/03b-000012-00g/collection-of-cyanobacteria-pcc). Cells were grown on solid or liquid BG11 media as described [17], with the exceptions that liquid cultures were grown in a shaking incubator at ambient CO_2 concentrations and antibiotics were added at the concentrations of 25 μg-ml^{-1} for kanamycin (km) and 120 μg-ml^{-1} for spectinomycin (Spc). Under these, non-CO_2-enriched conditions, the mean generation time was 32, 49, 45, 33, and 61 h for the F0, F3, F16, F3;16, and F30 strains, respectively.

Transformation of *S.* 6803 cells and propagation of transformants on selective media were as described [17].

The concentration of assayed metabolites is expressed in % DW. Conversion between OD_{750} and cell DWwas performed by regression analysis (Fig. S3).

2.3. Plasmids and gene constructs

Plasmids pUC4K [18], and pKRP13 [19] were kind gifts from Marcelo Tolmasky, CSU Fullerton, and Gregory Phillips, Iowa State University, respectively. Plasmids pUC57 and pUC57-simple were obtained from GenScript (GenScript Inc., USA). DNA constructs were designed using the MacVector software (MacVector Inc., USA) and synthesized by GenScript.

Plasmids (Figs. S4–S6) were constructed as described below. Codon optimization of heterologous genes for expression in *S.* 6803 were performed using the GenScript algorithms. Relevant plasmid sequences are shown in Figs. S7–S9. The introduced genes are controlled by strong *S.* 6803 promoters, P-*psbA2* for *FatB* and P-*rbcL* for the *FAR-FAD* operon. We used the *psbA2* gene as an integrative platform in the *S.* 6803 genome for both the *FatB* and FAR-FAD constructs. The *psbA2* gene encodes the photosystem II reaction center protein D1. We have previously shown [17,20] that insertional inactivation of *S.* 6803 *psbA2* upregulates a second *psbA* gene, *psbA3*, so as to restore D1 synthesis.

pFUEL3d: A 586 bp 5′ portion of the *S.* 6803 *psbA2* (locus *slr1311;* NCBI ID: 951890) gene, up to and including the start ATG codon, followed by the coding sequence (CDS) of the *FatB* gene from *Arabidopsis thaliana* (Accession NP_172327; NCBI ID: 837372)

Trait	Trait description	Gene constructs
3	TE with high activity for 16:0 and 18:0 FA-ACPs	*FatB* from *Arabidopsis thalaiana* (GenBank: NP_172327)
16	Inactivation of AAS activity	Insertional inactivation of *S.* 6803 *AAS* gene (locus *slr1609*)
30	Enhanced activity of FAR andFAD	Operon with *S.* 6803 *FAR* and *FAD* genes (loci *sll0208* and *sll0209*, respectively)

AAS: Acyl-ACP synthetase
ACC: Acetyl-CoA carboxylase
ACP: Acyl carrier protein
AGPAT: Acylglycerol-3-phosphate acyltransferase
CBB cycle: Calvin-Benson-Bassham cycle
DHAP: Dihydroxy-acetone phosphate
FA acyl-ACP: Fatty acyl-ACP
FAD: Fatty aldehyde decarbonylase
FAR: Fatty acyl-ACP reductase
FDH: Formate dehydrogenase
FFA: Free fatty acids
GPAT: Glycerol-3-phosphate acyltransferase
PHAS: Polyhydroxyalkanoate synthase
PHB: Polyhydroxybutyrate
TE: Thioesterase

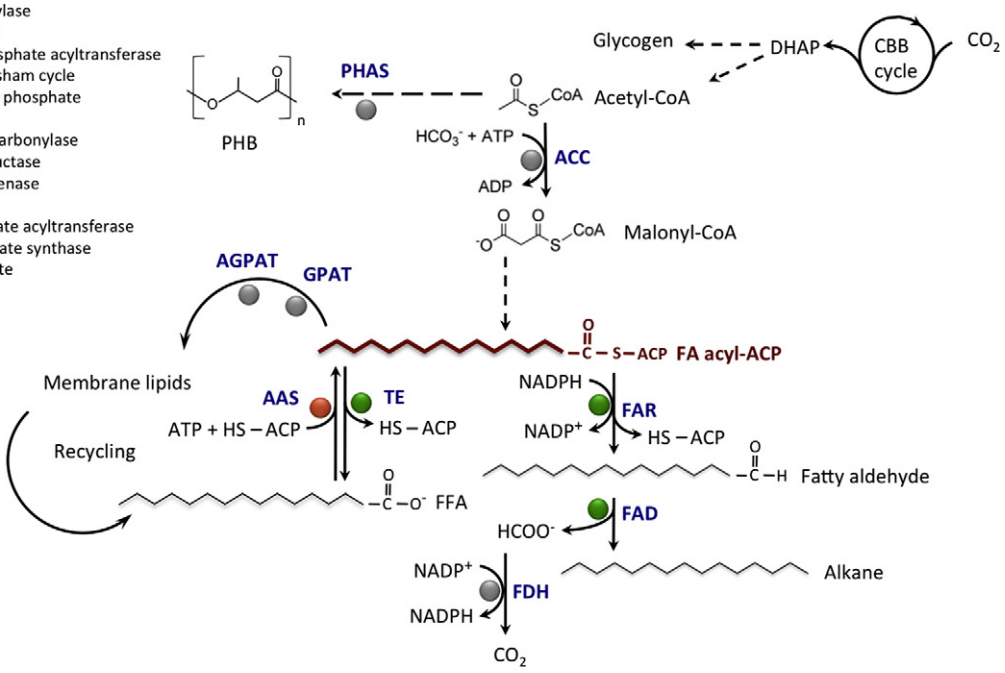

Fig. 1. Lipid metabolism in *S.* 6803-FUEL strains. Key enzymes affecting FA and alkane biosynthesis are shown (spheres). Enzyme activities targeted in this study are indicated with green for introduced/enhanced activities and red for blocked activity. Traits used to designate the strains are shown. The crossroad position of FA acyl-ACP in FA and alkane biosynthesis is indicated.

with the *S.* 6803 codon preference (e.g. http://exon.gatech.edu/metagenome/CodonUsageDatabase/?&page=16), and the 720 bp 3′ flanking region of *S.* 6803 *psbA2*, were designed as a contiguous sequence. An NdeI site encompassing the *psbA2* ATG start codon in the *psbA2-FatB* junction, a PstI site at the 5′ end, and a KpnI site at the 3′ end of the construct were added. The sequence was synthesized as an EcoRV fragment and blunt end cloned into pUC57-simple (GenScript). The resulting plasmid is referred to as pFUEL2. The km resistance gene, *nptII*, from pUC4K, including its own promoter, was released as a SalI fragment and cloned into SalI-digested pFUEL2, generating plasmid pFUEL3. To remove the endogenous NdeI site in the vector backbone, pFUEL3 was digested with ZraI and BstAPI, blunt ended with mung bean nuclease, and religated. This generated plasmid pFUEL3d.

pFUEL16: The *S.* 6803 *AAS* gene (locus *slr1609*; NCBI ID: 953643) was PCR amplified from genomic *S.* 6803 DNA using primers with Gateway-compatible extension (Invitrogen, USA) and cloned into the Gateway donor vector pDONR221 (Invitrogen). This resulted in plasmid pFUEL15. An Xma fragment from pKRP13, containing the streptinomycin/spectinomycin resistance cassette, was cloned into XmaI-digested pFUEL15, generating pFUEL16.

pFUEL30: The Gateway Frame A Cassette was inserted into SfoI-digested pFUEL3d, generating pFUEL29. The *sll0208* (NCBI ID: 952286) and *sll0209* (NCBI ID: 952637) loci in *S.* 6803, encoding the FAD and FAR enzymes, respectively, were assembled as an operon by utilizing the 5′ untranslated region (UTR) containing the −35 and −10 promoter signals, the first and third ribosome binding sites (RBSs), and the transcription termination signals of the *S.* 6803 *rbcLSX* operon. NotI, PacI, FseI, and SpeI sites were added. The construct was cloned as an EcoRV fragment in pUC57-simple. This plasmid is referred to as pFUEL23. The *sll0208-sll0209* operon from pFUEL23 was PCR amplified with Gateway primers and cloned into pFUEL29, replacing the Gateway cassette. This resulted in plasmid pFUEL30.

2.4. PCR

Phusion and OneTag DNA polymerases were used for cloning and colony PCR respectively. PCR reactions were carried out according to standard protocols.

2.5. Preparation of cells for single-cell SR-FTIR spectromicroscopy

Gold-coated glass slides were cut into 1.5 × 0.5 cm pieces using a diamond knife. The gold-coated slides were submerged in a series of washes for 5 min each: acetone, followed by sterile deionized water, 95% ethanol, and sterile deionized water. To ensure sterility, the gold-coated slides were autoclaved (121 °C for 20 min) three times, allowing a day between autoclaving to allow spores to germinate. The slides were functionalized with poly-L-lysine to facilitate cell adherence to the slide (100 μl of a 1/10 dilution of poly-L-lysine solution (P8920-100ML; Sigma Aldrich, USA) was applied to the slide immediately before use). The slides were coated for 1 h, and then rinsed three times with sterile deionized water.

Cells for SR-FTIR measurements were prepared using BG 11 medium and appropriate antibiotics. 1 ml of cell cultures in exponential phase was sampled and spun down twice for five minutes at 5000 rpm with fresh media to remove dead cells. Cells were then

resuspended in 300 μl fresh media and roughly 100 μl were dispersed onto the gold-coated slides and allowed to attach to the functionalized surface overnight at 30 °C with constant fluorescent light and ambient CO_2 concentrations and subsequently flooded with fresh medium. Immediately before the SR-FTIR spectromicroscopy measurements, cells (on the gold-coated slides) were first rinsed with Hanks' Buffered Saline Solution (HBSS) and then excess free-flowing HBSS was wicked away. Cells were then measured non-invasively and analyzed for their chemical composition.

2.6. SR-FTIR spectromicroscopy

All measurements were performed using a Nicolet Magna 760 FTIR bench and a Nicolet Nic-Plan IR microscope (Thermo Scientific, MA, USA) equipped with a microscope stage chamber at the infrared beamline of the Advanced Light Source (Lawrence Berkeley National Laboratory, CA, USA; http://infrared.als.lbl.gov/). The numerical aperture of the objective of the infrared microscope was 0.65. The location of the synchrotron infrared beam within the field of the microscope was fiducialized to a 1-μm accuracy by mapping a titanium on a silicon calibration target. During the measurements, photons emitted over a mid-infrared wavenumber range of 4000–800 cm^{-1} from the synchrotron were focused by the all-reflective optics infrared microscope through the cells onto the gold-coated reflective surface. We visually identified and marked the locations of the cells before raster scanning, collecting full SR-FTIR transflectance spectra at each position using a single-element MCT detector. In transflectance, the synchrotron infrared beam transmitted through the cells, reflected off the gold-coated surface, and then transmitted through the sample a second time before reaching the detector. Each spectrum was collected at a spectral resolution of 4 cm^{-1} with eight co-added scans and a peak position accuracy of 1/100 cm^{-1}. Background spectra were acquired from neighboring locations without any cells, and used as reference spectra for both samples and standards to remove background H_2O and CO_2 absorptions. The following data processing and analysis were used to interrogate metabolic alternations in engineered *S.* 6803 for biosynthesis of free FA.

2.7. SR-FTIR data processing and multivariate analysis

All SR-FTIR transflectance spectra were subjected to an array of data preprocessing and processing calculations using Thermo Electron's Omnic version 7.3. The processing includes the computation conversion of transflectance to absorbance, spectrum baseline removal, and statistical analysis. The absorption spectra show clear signatures of free fatty acids, proteins, lipids, and polysaccharides (Fig. 2).

Baseline corrected and vector-normalized spectra in the biochemical fingerprint region between 4000 and 1000 cm^{-1} (Fig. S10) were then subjected to the multivariate principal component analysis (PCA) and then linear discriminant analysis (LDA) using MathLab (7.0). PCA and LDA were used to generate new variables (factors) that were linear combinations (i.e. weighted sum) of the original variables (wavenumbers). PCA was applied to the spectra first to reduce the hundreds of absorbance intensities at different wavenumbers to just a few factors that could capture more than 95% of the variance. We typically selected seven components based on the 95% percentage of variance explained and on the spectral features of the loading plot. LDA was then applied to maximize the "inter-class" variance over the "intra-class" variance of the factors. We visualized the multivariate analysis results in the form of score plots and cluster vector plots (Fig. 2). In this study, score plots were 2- and 3-dimensional plots where the first three PC-LDA components were the *x*-, *y*- and *z*-axes; the nearness between classes (clusters) indicates the similarity, whereas the distance between classes implies dissimilarity. The cluster vectors plots [21] were 2D plots where the *x*-axis is in wave number units, and the *y*-axis depicts the cluster vectors coefficient values of engineered strains relative to the F0 control strain. The PC-LDA loadings determined the wavenumbers (modes of vibrations) responsible for segregation of classes. The loadings plots were 2D plots where the *x*-axis is in wave number units, and the *y*-axis depicts the loadings coefficient values (Fig. S1).

2.8. GC/MS analyses

Free Fatty Acids (FFAs), phospholipids (PLs) and alkanes were quantified by extraction of pellets from cells harvested at OD_{750} = 0.6 by the Bligh–Dyer method [22–25]. Briefly, 10 ml of a 10:5:4 mixture of methanol:chloroform:pH 7 phosphate buffer was combined with the samples. Three internal standards, 1,2-dinonadecanoyl-sn-glycero-3-phosphocholine (Avanti Polar Lipids, Alabaster, Alabama), dodecanoic acid, and eicosane (Sigma Aldrich, St. Louis, MO) were added as controls. The mixture was vortexed, sonicated for 2 min and extracted at room temperature in the dark for 3 h. Phases were separated with the addition of 2 ml of chloroform and 2 ml of water, vortexed, and centrifuged at 2000 rpm for 15 min to separate the organic and aqueous layers. The organic layer was removed and dried under N_2 and the FFAs and alkanes were separated from the PLs on a C-18 silica column (Sigma Chemicals, St. Louis, MO) by elution first with chloroform with 50 μL of glacial acetic acid added to collect the free fatty acids followed by methanol to elute PLs. Both fractions were dried under N_2 and subjected to a acid hydrolysis by resuspending with 10:1:1 methanol:chloroform:concentrated HCl, vortexed for 2 min and incubated in a water bath at 60 °C for 15 h. This procedure methylates both the FFA and PL to fatty acid methyl esters (FAMEs). The resulting FAME compounds were extracted with 3 × 2 ml of hexane, and dried under N_2. A 50 μL of 46.2 mg/L methyl undecanoate (Sigma Chemicals, St. Louis, MO) was added to the dried extracts as an external standard. The resultant FAME and alkane compounds were detected on an Agilent 6890 GC/MS.

2.9. NMR analysis

Results were obtained on the methanol:water (5:4 v/v) fraction from the cell extraction protocol (stored at −20 °C). The top 6 ml of each sample were placed in a 50 ml Falcon tube, and 14 ml of water were added prior to lyophilizing the sample (to prevent methanol boil off). The samples were lyophilized for approximately 24 h, and subsequently dissolved in a mixture of 500 μl of deuterated methanol and 400 μl deuterium oxide. Each sample was vortexed and centrifuged briefly. 700 μl of this resuspended sample was then transferred into an eppendorf tube, and 20 μl of a 0.42 mM trimethylsilyl propanoic acid (TSP) was added for reference. Finally, 600 μl of the final mixture were placed into a 5 mm NMR tube. All of the spectra shown here were acquired on an 800 MHz ^1H frequency Bruker NMR spectrometer.

3. Results

We have generated a suite of *S.* 6803 strains aimed for FFA and alkane production. Here we describe four of these *S.* 6803-FUEL strains, F3, F16, F3;16, and F30 (Fig. 1). Strain F3 contains a codon-optimized *TE* gene encoding the Arabidopsis *FatB* sequence. The Arabidopsis FatB TE shows preference for 16:0 and 18:0 FA acyl-ACPs, and thus would be expected to yield *S.* 6803 cells producing 16:0 and 18:0 FFAs. Additionally, the concomitant decrease in acyl-ACP levels should also relieve the rigorous feedback inhibition of acetyl-CoA carboxylase (ACC; EC 6.4.1.2) (and other

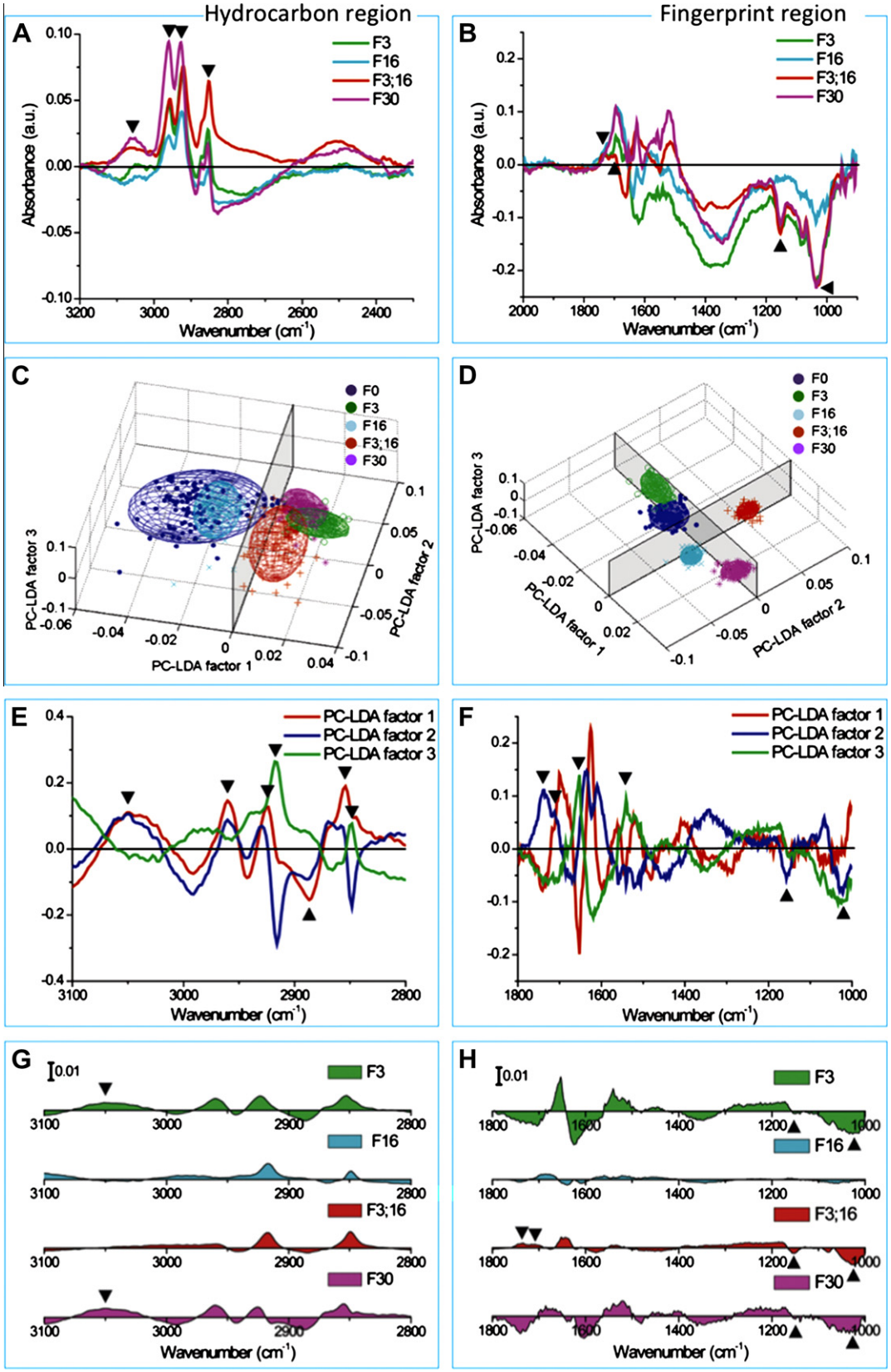

Fig. 2. Infrared spectroscopy analysis of phototrophic productions of biofuels in Cyanobacteria in the hydrocarbon and the fingerprint spectral regions. (A and B) The mean difference spectrum between the engineered strains and the F0 control in (A) the hydrocarbon region (3100–2800 cm^{-1}) and (B) the biomolecular fingerprint region. (C and D) Exploratory 3D PC-LDA of populations of the strains in the two spectral regions. The partitions are for improved viewing. Two-by-two 2D comparisons of the PC-LDA plots are shown in *Fig.* S1. (E and F) The first three PC-LDA loadings of the complete data set in the two spectral regions. (G and H) Cluster vector plots (F0 as comparator) for the two spectral regions. Arrows: markers of spectral features for metabolic shifts and productions of biofuels. See text for peak locations.

FA-biosynthesis enzymes) exerted by this end product [2]. In strain F16, the *S.* 6803 *AAS* gene, encoding the enzyme acyl-ACP synthase is inactivated. The purpose with this maneuver is to prevent re-thioesterification of FFAs to FA acyl-ACPs. Thus FAs formed via recycling of membrane lipids will not find their way into the acyl-ACP pool. Strain F3;16 contains both the 3 and 16 trait. Strain F30 contains one extra copy each of the *S.* 6803 *FAR* and *FAD* genes assembled as an operon. The increased activity of the FAR and FAD enzymes would be expected to result in enhanced alkane production. This may also provide a stronger sink for FA acyl-ACPs and, hence, further increase the carbon flux from acetyl-CoA toward FAs. The control strain of *S.* 6803 is referred to as F0.

3.1. Single-cell SR-FTIR metabolic fingerprinting

Alternations in metabolism of the *S.* 6803-FUEL strains were investigated using SR-FTIR spectromicroscopy. The aim here was to exploit the high-resolution SR-FTIR spectromicroscopy as a high-throughput (150 cells in 20 min) analytical tool for collecting multiplex metabolic information from individual engineered cells. The spectral information was stored and subsequently deconvoluted and dissected in greater detail. In this study, we focused on key absorption bands throughout two spectral regions: the hydrocarbon region (3100–2800 cm^{-1}) and the biomolecular fingerprint region (1800–1000 cm^{-1}). Individual mean and difference absorption spectra are shown in Figs. 2A and B and S1. Their molecular assignments are summarized in Table S1. At least 100 single cells were measured for each strain. The multivariate principal component and linear discriminant analysis (PC-LDA) of individual spectra for each cell reveal the following molecular information.

1. In the hydrocarbon region (3100–2800 cm^{-1}), the three-dimensional score plot revealed that F3, F3;16, and F30 are separated from F16 and F0 by the first PC-LDA factor (Figs. 2C and S1-A). The loadings of this factor (the red trace in Fig. 2E) reveal that the positive features near 3049 cm^{-1}, 2960 cm^{-1}, 2924 cm^{-1} and 2854 cm^{-1}, and the negative feature near 2887 cm^{-1} are responsible for the separation. When compared with the difference spectrum for each strain (Fig. 2A), the loading features near 3049 cm^{-1} co-located with the absorption band that can be assigned to the CH vibration in alkenes of hydrocarbons (Table S1); whereas the loading features near 2960 cm^{-1}, 2924 cm^{-1} and 2854 cm^{-1} co-located with absorption bands that can be assigned to CH_2 and CH_3 stretching vibrations of saturated hydrocarbon chains. The overall PC-LDA1 scores of the F3, F3;16, and F30 strains are positive (Fig. 2C), reflecting a relative abundance in hydrocarbons compared to the F16 and F0 strains. The cluster vector plots for each engineered strain (Fig. 2G), which reflect its difference from F0, show that only the F30 and F3 strains exhibit increasing absorption near 3049 cm^{-1} that could be assigned to alkene-like hydrocarbons (Table S1).
2. In the biomolecular fingerprint region (1800–1000 cm^{-1}), the 3D score plot shows a more intricate clustering pattern (Fig. 2D). The first PC-LDA factor separates strains F0 and F3 from F3;16, F16, and F30; the second PC-LDA factor further separates strain F3;16 from F16 and F30; while the third PC-LDA factor separate F0 from F3 (Figs. 2D and S1B). The loadings of the first factor (red[1] trace in Fig. 2F) show that the protein structures amide I (between 1700–1600 cm^{-1}) and amide II (between 1580–1510 cm^{-1}) are responsible for the separation. The loadings of the second factor (blue trace in Fig. 2F) show that the positive features near 1738 cm^{-1} and 1712 cm^{-1} in the ester and FFA carbonyl region (1700–1780 cm^{-1}), respectively, play a key role in discriminating F3;16 from F16 and F30. The loadings of the third factor show that the negative feature near 1157 cm^{-1} and 1022 cm^{-1} in the region for glycogen and other polysaccharides is responsible for the separation. Similarly, the cluster vector plots (Fig. 2H) together with the difference spectra (Fig. 2B) reveal that the positive feature, which is present only in F3;16, could arise from the vibrations of the C=O near 1738 cm^{-1} in PHAs [26] and the C=O near 1712 cm^{-1} in FFA [27]. In contrast, the negative features near 1157 cm^{-1} and 1022 cm^{-1} arise from the vibrations of glycosidic bonds and the C—O—C and C—O—P bonds of glycogen [28,29] (Table S1). A close comparative examination of the cluster vector plots shows that the overall polysaccharide features in all engineered strains decreased relative to the F0.

3.2. Bulk measurements by GC/MS/NMR

3.2.1. Alkane biosynthesis

The pathway for alkane synthesis in cyanobacteria seems to proceed via decarbonylation of fatty aldehydes [12], the major route for alkane synthesis in most organisms [30]. Gene sequences for *FAR* and *FAD* have recently been identified from several cyanobacteria [12]. Interestingly, the decarbonylation step in cyanobacterial alkane biosynthesis may involve the release of formate ($HCOO^-$) rather than CO, which has been the assumed coproduct in alkane biosynthesis [31] (Fig. 1). The physiological role(s) of alkanes in cyanobacteria is unknown. Not all cyanobacteria synthesize alkanes and in those that do, alkanes accumulate in very small amounts. It is possible that alkanes are required for proper membrane fluidity or function. Although heptadecane (C17) is the predominant *n*-alkane among cyanobacteria, many strains synthesize a wide array of linear, branched, and cyclic alkanes, some of which (e.g. branched methyl- and ethylalkanes) may be unique to cyanobacteria [2,32]. For example, the cyanobacterium *Microcoleus* produces four *n*-alkanes and more than 60 different branched alkanes [32].

Analysis of cellular extracts from strain F0 showed that *S.* 6803 produces heptadecane and, to a much lesser extent, the alkene 9-heptadecene (Fig. 3A). The levels of both heptadecane and 9-heptadecene were significantly enhanced in strain F30 containing the *FAR-FAD* operon. This holds promise for further optimizing alkane yield in cyanobacteria by continued pathway engineering, e.g. increasing carbon flux upstream of FA acyl-ACP.

Also the F3;16 strain showed enhanced levels of heptadecane. This finding is counterintuitive since both the "3" and "16" traits would be expected to decrease the size of the acyl-ACP pool (Fig. 1), a notion that is reinforced by the results from the F3 and F16 strains, where the heptadecane levels remained unaffected, or were slightly decreased. Why the F3;16 strain had increased accumulation of heptadecane is not obvious. It should be cautioned, however, that this strain exhibited great variability in heptadecane levels between samples, and thus attempts at finding a possible explanation may be premature.

To reveal a possible bottleneck in the flux of carbon through the FAR and FAD enzymes, we looked for accumulation of octadecanal, the FA aldehyde substrate for FAD, in the F30 strain. No such compound was detected in any of the strains, although low levels of octadecenal species were found in F3;16 but were virtually undetectable in the other strains (Fig. 3B).

3.2.2. Intracellular FAs

Contrary to expectation, strain F3 showed no increase in the amounts of intracellular FFA (Fig. 4). Strain F16 showed a modest but notable increase, and strain F3;16 demonstrated a dramatic

[1] For interpretation of color in Fig. 2, the reader is referred to the web version of this article.

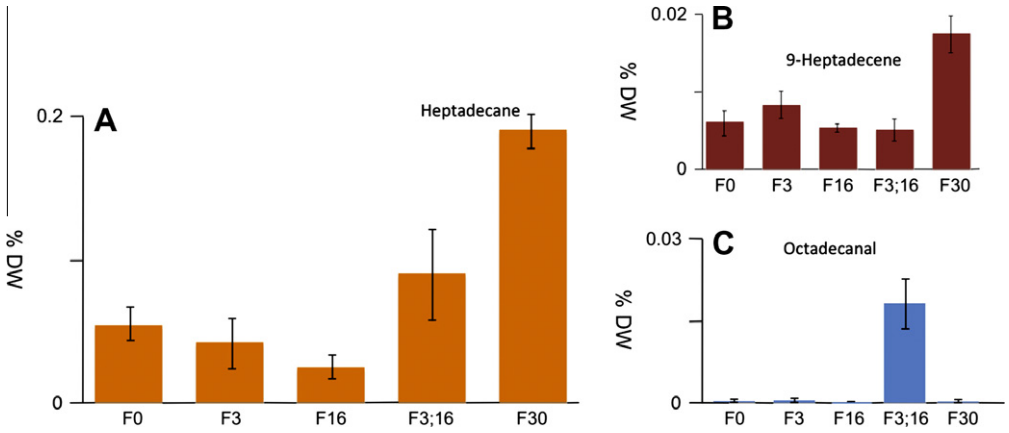

Fig. 3. Hydrocarbon (A) and aldehyde (B) levels in cell pellets from *S.* 6803 cultures. Data were obtained from biological triplicates.

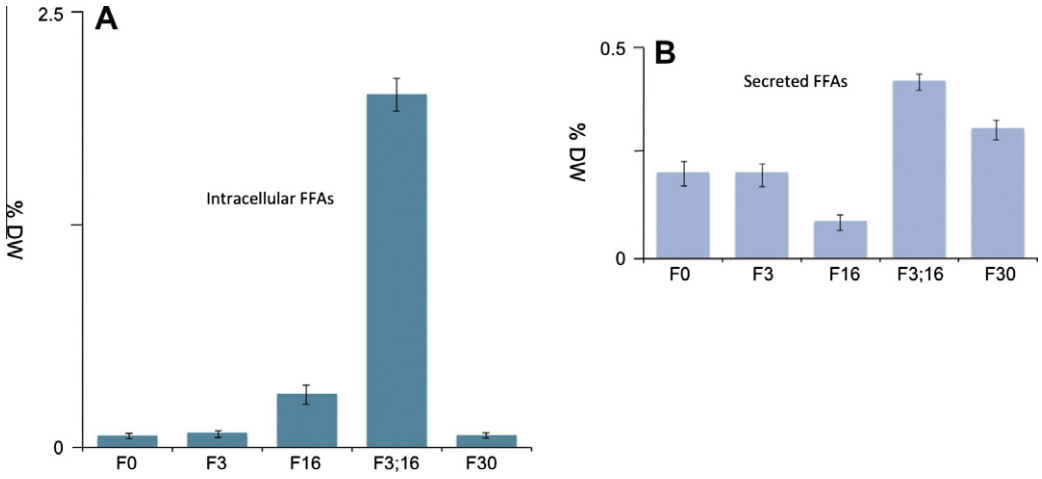

Fig. 4. Levels of total intracellular or secreted FFAs from *S.* 6803 cultures. Data were obtained from biological triplicates.

30-fold rise in FFA levels. No increase in FFAs was observed in the F30 strain. The reason for the low levels of FFAs in F3 could be because of one or more of three possibilities; (i) the AAS enzyme is efficient enough to compensate for the introduced TE activity, (ii) the majority of the FFAs was secreted to the culture medium, or, (iii) the introduced TE enzyme is non-functional. The latter alternative is less likely, given the strikingly different phenotypes between the F3 and F3;16 strains. Also, although the amount of FFAs found in the culture medium of the F3 strain was approximately twice that which remained in the cells, the same was true for the F0 strain (see below). Thus this also does not seem to explain the lack of increase in FFAs levels in the F3 strain. Rather, we are left with the conclusion that a plausible reason for the lack of increased FFA levels in the F3 strain is because a high activity of the AAS enzyme masks the liberation of FFAs from the acyl-ACP pool. In other studies on *S.* 6803 it was reported that most of the FFAs produced by the presence of a TE and/or absence of the AAS were secreted, and that secretion of FFAs in the control strains was insignificant [4] and Kaczmarzyk and Fulda [10]. Our results differ in this respect since the F0 strain showed a roughly equal distribution of intracellular and secreted FFAs. Also, although the F3;16 strain secreted twice as much FFAs as F0, the proportion of intracellular/secreted FFAs was higher in F3;16 than in F0, due to the large total increase in FFAs. The reason for this discrepancy between studies could be different culture conditions (we used gentle shaking with ambient CO_2), or because of different variants of the *S.* 6803 strain (we used the non-G strain [33]). In agreement with the conclusion above, the difference in FFA production between F3;16 and F16 is indicative of the TE activity, while the difference between F3;16 and F3 suggests a high AAS activity.

An inspection of the intracellular FFAs in the F3;16 strain shows a predominance of stearic acid (octadecanoate; 18:0) and palmitic acid (hexadecanoate; 16:0), with the remainder being mostly mono-unsaturated octadecanoates, primarily oleic acid (18:1 Ω9), vaccenic acid (18:1 Ω7) and euric acid (22:1 Ω9) (Fig. 5). Cyanobacterial acyl-ACPs are all saturated and desaturases in cyanobacteria act exclusively on lipids [34], and, therefore, unsaturated FFAs are likely to be derived from recycling of membrane lipids. This would explain the different FFA profiles between F3;16 on one hand, and F0, F3 and F30 on the other; in F3;16, where the *AAS* gene has been inactivated, the conversion of recycled FAs from membrane lipids to acyl-ACPs has been disrupted, resulting in an accumulation of unsaturated FFAs. It must be emphasized that the FFA distribution displayed in Fig. 5B only serves to show relative amounts for a specific strain; as is shown in figures 3 and 4A, the total amounts of FFAs in F0, F3 and F30 are very small. The high levels of 16:0 and 18:0 FFAs in F3;16 are due to the presence of the Arabidopsis FatB TE, which has a substrate preference for 16:0 and 18:0 FA acyl-ACPs. The FatB TE exhibits the strongest affinity for 16:0 FA acyl-ACPs, which is reflected in the higher proportion of 16:0 over 18:0 FFAs in F3. On the other hand, the lack of noticeable 16:0 FFAs in F3 again points

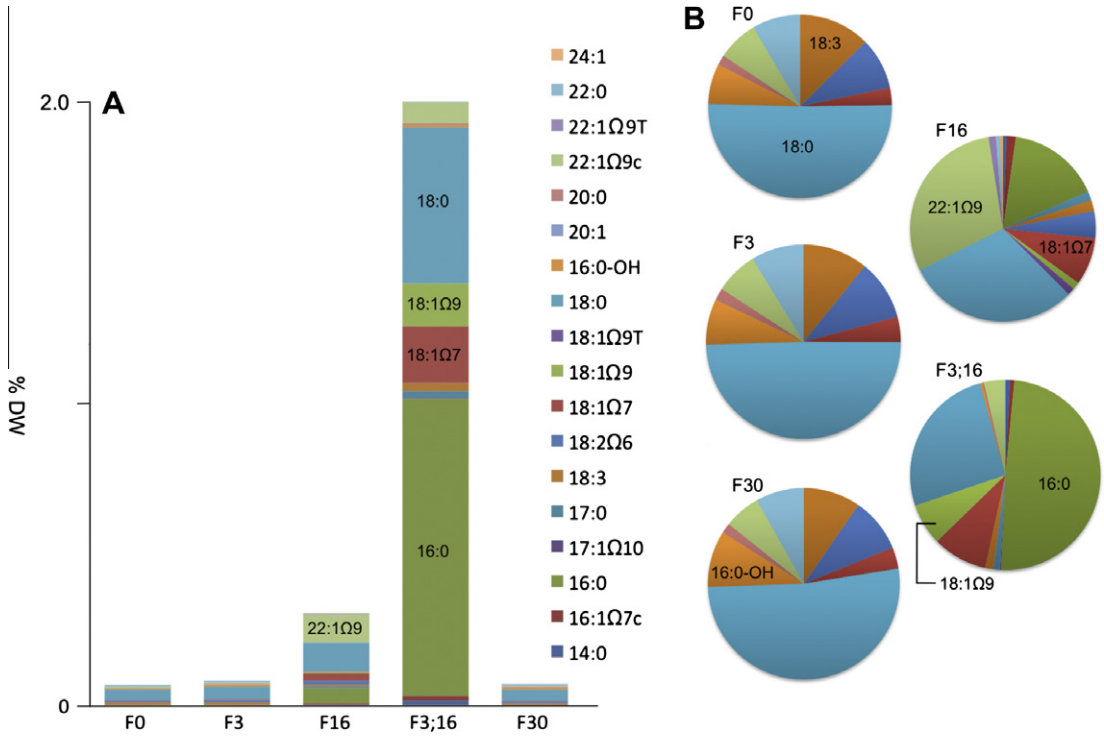

Fig. 5. Composition of the intracellular FFA pool. (A) The relative amounts of FFAs between the different strains, (B) the relative amounts of different FFAs in each strain. Data were obtained from biological triplicates.

to a high activity of the AAS enzyme, which apparently very efficiently re-thioesterifies FFAs generated by the introduced TE enzyme.

3.2.3. Secreted FAs

The composition of FFAs secreted by the F3;16 cells differed significantly from the intracellular pool, with the majority being unsaturated, chiefly linoleic acid (18:2 Ω9), palmitoleic acid (16:1 Ω7), vaccenic acid (18:1 Ω7) and α-linoleic acid (18:3 Ω3) derived from membrane lipid degradation (Fig. 6). Similar to the intracellular pool of FFAs in F3;16, the activity of the TE enzyme manifested itself in the over 4-fold higher amount of secreted FFAs for the F3;16 strain compared to the F16 strain. The reason for the higher unsaturated/saturated FFA ratio in the secretion products, which is also evident for the F0, F3 and F16 strains, is not clear but may be due to a preference in the secretion process for unsaturated over saturated FAs [10]. The F30 strain deviated from the general observation of a high proportion of unsaturated FA in the secreted FFA pool by showing relatively high amounts of stearic and palmitic acids, which contributed to the high levels of total FFAs secreted from this strain (Fig. 4). We find it difficult to reconcile these results with the enhanced FAR and FAD activities in F30, which increased the flux of 18:0 acyl-ACP toward heptadecane biosynthesis.

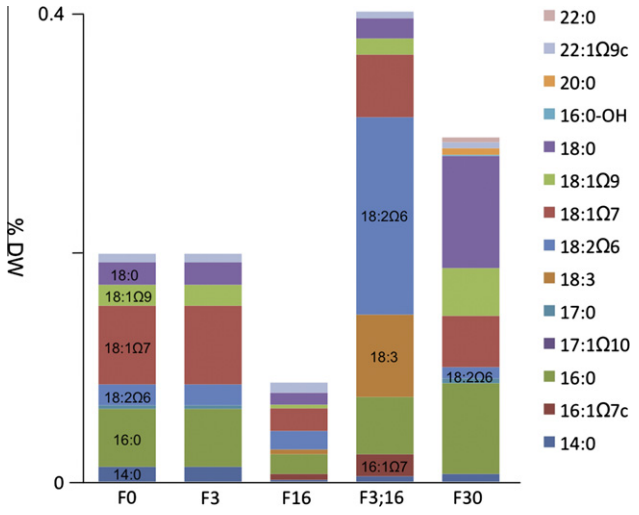

Fig. 6. Secreted FFAs. The relative amounts of the FFAs between different strains are shown. Data were obtained from biological triplicates.

3.2.4. Hydroxylated FAs

Selected compounds detected in the phospholipid fraction of the *S.* 6803 strains are listed in Table S2. In accordance with the study by Murata and colleagues, e.g., [35], our results show that lipids of *S.* 6803 have a high 16:0/18:0 FA ratio. One notable finding from the phospholipid analysis is the elevated levels of two hydroxylated FAs, 3-OH stearic acid (3-OH 18:0) and 3-OH myristic acid (3-OH 14:0) in the F16 and F3;16 strains (Fig. 7A). These FAs are known constituents of lipid A, a component of the lipopolysaccharide (LPS, also referred to as "endotoxin") of the outer membrane of Gram-negative bacteria [36]. Hydroxylated FAs are rarely found in any other lipids in Gram-negative bacteria and we assume that the 3-OH 18:0 and 3-OH 14:0 detected in the *S.* 6803 strains were extracted from the outer membrane. The higher amounts of these FAs in the F16 and F3;16 strains compared to F0 may either be indicative of an increased *de novo* synthesis of 3-OH stearic acid and 3-OH myristic acid and possibly increased formation of lipid A, or an accumulation of 3-OH stearic acid and 3-OH myristic acid as partly degraded outer membranes. The levels of 3-OH stearic acid were higher in F3;16 than in F16, suggesting the release of 18:0 FFAs from the acyl-ACP pool by the TE enzyme with subsequent hydroxylation. This link, between production of FFAs and accumulation of 3-OH FAs, in turn, indicate that *de novo*

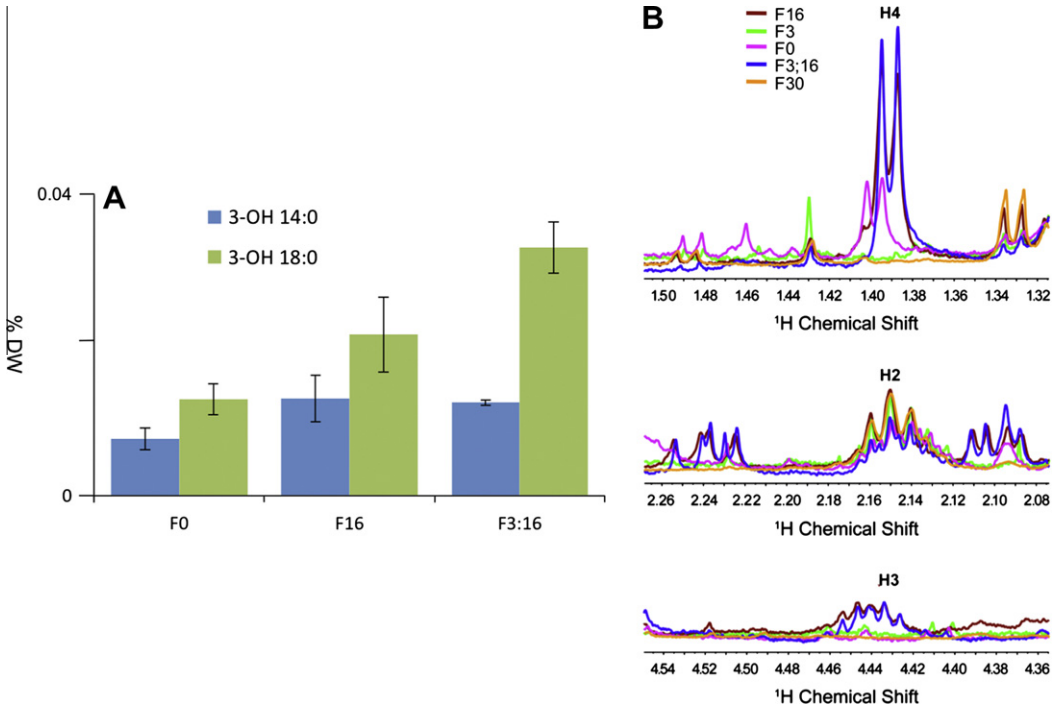

Fig. 7. Levels of 3-OH FAs as determined by GC/MS (A) and NMR (B). (A) Amounts of 3-OH stearic and 3-OH myristic acid. (B) Expansions of different regions of the ^{1}H 1D NMR spectra showing the presence of 3-OH butyric acid. Data were obtained from biological triplicates.

synthesis of 3-OH stearic and myristic acids at least partially accounts for their increased amounts in the F3;16 strain.

Another 3-OH FA, 3-OH butyrate (3-OH 4:0; ß-OH butyrate), was detected as a significant signal in 1-dimensional ^{1}H NMR spectra in extracts from the F16 and F3;16 strains but was below detection limits in the other strains (Fig. 7). The identity of the compound as 3-OH butyrate was confirmed with 2D spectra (Fig. S2). A distinguishing feature of 3-OH butyrate is as a precursor in the biosynthesis of polyhydroxybutyrate (PHB), a polyhydroxyalkanoate (PHA) produced by *S.* 6803 and several other bacteria as an energy and carbon storage compound.

4. Discussion

Our SR-FTIR observations in the hydrocarbon region clearly demonstrate an increase in the accumulation of hydrocarbons in strains F3, F3;16 and F30 strains in comparison to F0 (Fig. 2A, C, E, and G). This agrees with the accumulation of heptadecane and 9-heptadecene in F30 (Fig. 3), the elevated levels of 9-heptadecene in F3 (Fig. 3), and the accumulation of FFAs and the elevated levels of heptadecane and octadecenal in F3;16 (Figs. 3 and 4). It is noteworthy that the distinct phenotypic separation between F3 and F0 in the PC-LDA1 scores (Figs. 2C and S1A) corresponds to only minor observable differences in the GC/MS analyses, i.e., a slightly higher amount of 9-heptadecene and a slightly lower amount of heptadecane in F3 (Fig. 3. In fact, from the GC/MS analyses, the properties of F3 are mainly revealed in the context of the F3;16 background.

Also in the SR-FTIR fingerprint region, the F3 strain clearly segregates from the F0 strain, mainly due to the decrease in glycosidic bonds (Figs. 2D, H and S1B). Glycosidic bonds are decreased also in the F3;16 and F30 and, to a lesser extent, F16 strains (Fig. 2B and H). Polysaccharides such as glycogen and exopolysaccharide substances (EPSs) are prominent compounds in cyanobacteria, and the data suggest that portions of the carbon flux in the engineered strains has shifted from polysaccharide biosynthesis in favor of being shunted to acetyl-CoA (Fig. 1). Although exhibiting similar negative peaks for polysaccharides in the difference spectra (Fig. 2B), F3;16 and F30 were clearly phenotypically separated by the second PC-LDA factors (Fig. 7D). This reflects the large increase in F3;16 of carbonyl groups in FAs and PHA (Fig. 2B and H; Table S1). The increase in FAs is consistent with the accumulation of FFAs (Fig. 4) and 3-OH stearic and 3-OH butyric acid (Fig. 7). The presence of carbonyl groups as carboxyl esters in PHA implies that the 3-OH butyric acid was used for PHA biosynthesis. Although we do not know the mechanisms, it is conceivable that the accumulation of FFAs in F3;16 signals a metabolic imbalance that triggers a shift in the utilization of acetyl-CoA from FA synthesis to formation of PHB. No PHA was detected in the F16 strain, although it also accumulated 3-OH butyric acid (Figs. 2C and 7). The separation of strains by the first PC-LDA factor is to a large extent caused by differences in the amount and nature of protein secondary structures and can be attributed to the altered composition of enzymes that results from the engineering steps.

Each data point in the PC-LDA plots in Fig. 2C and D represents one cell. Thus although the strains segregate in phenotypic populations, a great deal of metabolic heterogeneity exists within each strain, including the F0 control. It is becoming increasingly clear that such cell-to-cell variation in isogenic microbial populations is stochastic in nature [37–39], and that this heterogeneity to a major extent dictates how the population responds to perturbations such as environmental stress or to metabolic engineering.

As pointed out by Lidstrom and Konopka [37], if only a small subset of cells in a population of an engineered strain exhibits a certain trait, such as high-yield production of a desirable metabolite, simply overexpressing the target pathway in the bulk population is unlikely to increase the proportion of high producers. Rather, by appreciating that the monitored trait of the population (i.e., high productivity), is dominated by a subpopulation, we have a better chance at increasing the number of high producers by understanding the mechanisms by which these cells differ from

the rest in the population. For example, FTIR analysis is consistent with the GC/MS measurements in showing that the bulk of the F0 population contains low amounts of hydrocarbons. Moreover, the PC-LDA scores also reveal that some F0 cells exhibit higher hydrocarbon levels (Fig. 2C). Indeed, some cells overlap with the lower end of the F30 population. As another example, the F30 and F3;16 populations harbor cells with positions at the lower end of the 2nd dimension in Fig. 2C, probably indicating deviation in the details of the hydrocarbon structures, such as branching.

5. Conclusions

We have demonstrated a simple high-throughput single-cell SR-FTIR approach for rapidly examining the metabolic profiles of *S.* 6803 strains engineered for enhanced phototrophic production of alkanes and FFAs. SR-FTIR data showed accumulation of functional groups in agreement with the GC/MS/NMR results. SR-FTIR data also could demonstrate a shift in carbon utilization from polysaccharide to lipid-based metabolism and to PHB biosynthesis. Finally, multivariate analysis of FTIR spectra revealed that the different strains were phenotypically segregated, but that the stochasticity in the populations gave rise to a high degree of cell heterogeneity within the population for each strain. These findings point to the importance of single-cell approaches to unravel the mechanisms that control specific traits in individual cells. Since SR-FTIR spectromicroscopy is a non-invasive tool, cells can be selected for downstream processing and omic investigation based on FTIR data. We suggest that our results demonstrate the applicability of SR-FTIR spectromicroscopy as a powerful means for metabolic screening and phenotyping of live individual cells.

Acknowledgements

This work was supported by the US Department of Energy Office of Biological and Environmental Research's Structural Biology (BSISB) Program through contract DE-AC02-05CH11231 with Lawrence Berkeley National Laboratory. The SR-FTIR spectromicroscopy work was conducted at the infrared beamline at the Advanced Light Source, which is supported by the Director, Office of Science, Office of Basic Energy Sciences, of the US Department of Energy. Funding from a Laboratory Directed Research and Development (LDRD) grant (CyanoAlkanes) to C.J. is acknowledged.

Appendix A. Supplementary data

Supplementary data associated with this article can be found, in the online version, at http://dx.doi.org/10.1016/j.apenergy.2012.08.047.

References

[1] Ducat DC, Way JC, Silver PA. Engineering cyanobacteria to generate high-value products. Trends Biotechnol 2011;29:95–103.
[2] Jansson C. Metabolic engineering of cyanobacteria for direct conversion of CO_2 to hydrocarbon biofuels. Progress in Botany 2012;73:81–93.
[3] Jansson C. Employing cyanobacteria for biofuel synthesis and CCS, In: Radu R, editor. Solar energy. Rijeka, Croatia: InTech; 2012. p. 367–78.
[4] Liu XY, Sheng J, Curtiss R. Fatty acid production in genetically modified cyanobacteria. Proc Natl Acad Sci USA 2011;108:6899–904.
[5] Quintana N, Van der Kooy F, Van de Rhee MD, Voshol GP, Verpoorte R. Renewable energy from cyanobacteria: energy production optimization by metabolic pathway engineering. Appl Microbiol Biotechnol 2011;91:471–90.
[6] Ruffing AM. Engineered cyanobacteria: teaching an old bug new tricks. Bioeng Bugs 2011;2:136–49.
[7] Campbell JW, Cronan JE. Bacterial fatty acid biosynthesis: targets for antibacterial drug discovery. Ann Rev Microbiol 2001;55:305–32.
[8] Cronan JE. Bacterial membrane lipids: where do we stand? Ann Rev Microbiol 2003;57:203–24.
[9] Voelker T, Kinney AT. Variations in the biosynthesis of seed-storage lipids. Ann Rev Plant Phys 2001;52:335–61.
[10] Kaczmarzyk D, Fulda M. Fatty acid activation in cyanobacteria mediated by acyl–acyl carrier protein synthetase enables fatty acid recycling. Plant Physiol 2010;152:1598–610.
[11] Nawabi P, Bauer S, Kyrpides N, Lykidis A. Engineering *Escherichia coli* for biodiesel production utilizing a bacterial fatty acid methyltransferase. Appl Environ Microb 2011;77:8052–61.
[12] Schirmer A, Rude MA, Li XZ, Popova E, del Cardayre SB. Microbial biosynthesis of alkanes. Science 2010;329:559–62.
[13] Naumann D. Infrared spectroscopy. In: Meyers RA, editor. Microbiology, Encyclopedia of analytical chemistry. Chichester, U.K: John Wiley & Sons Ltd.; 2000.
[14] Holman H-YN, Bechtel HA, Hao Z, Martin MC. Synchrotron IR spectromicroscopy: chemistry of living cells. Anal Chem 2010;82:8757–65.
[15] Holman HYN, Wozei E, Lin Z, Comolli LR, Ball DA, Borglin S, et al. Real-time molecular monitoring of chemical environment in obligate anaerobes during oxygen adaptive response. Proc Natl Acad Sci USA 2009;106:12599–604.
[16] Llabjani V, Trevisan J, Jones KC, Shore RF, Martin FL. Binary mixture effects by PBDE congeners (47, 153, 183, or 209) and PCB congeners (126 or 153) in MCF-7 cells: biochemical alterations assessed by IR spectroscopy and multivariate analysis. Environ Sci Technol 2010;44:3992–8.
[17] Jansson C, Salih G, Eriksson J, Wiklund R, Ghebramedhin H. Use of *Synechocystis* 6803 to study expression of a *psbA* gene family. Methods Enzymol 1998;297:166–82.
[18] Vieira J, Messing J. The Puc plasmids, an M13mp7-derived system for insertion mutagenesis and sequencing with synthetic universal primers. Gene 1982;19:259–68.
[19] Reece KS, Phillips GJ. New plasmids carrying antibiotic-resistance cassettes. Gene 1995;165:141–2.
[20] Jansson C, Debus RJ, Osiewacz HD, Gurevitz M, Mcintosh L. Construction of an obligate photoheterotrophic mutant of the Cyanobacterium *Synechocystis* 6803 – inactivation of the *Psba* gene family. Plant Physiol 1987;85:1021–5.
[21] Llabjani V, Trevisan J, Jones KC, Shore RF, Martin FL. Binary mixture effects by PBDE congeners (47, 153, 183, or 209) and PCB congeners (126 or 153) in MCF-7 cells: biochemical alterations assessed by IR spectroscopy and multivariate analysis. Environ Sci Technol 2010;44:3992–8.
[22] Guckert JB, Antworth CP, Nichols PD, White DC. Phospholipid, ester-linked fatty-acid profiles as reproducible assays for changes in prokaryotic community structure of estuarine sediments. Fems Microbiol Ecol 1985;31:147–58.
[23] Guckert JB, Ringelberg DB, White DC, Hanson RS, Bratina BJ. Membrane fatty-acids as phenotypic markers in the polyphasic taxonomy of methylotrophs within the proteobacteria. J Gen Microbiol 1991;137:2631–41.
[24] Pfiffner SM, Cantu JM, Smithgall A, Peacock AD, White DC, Moser DP, et al. Deep subsurface microbial biomass and community structure in Witwatersrand Basin mines. Geomicrobiol J 2006;23:431–42.
[25] White DC, Ringelberg DB. Signature lipid biomarker analysis. In: Techniques in microbial ecology; 1998. p. 255–72.
[26] Hong K, Sun S, Tian W, Chen GQ, Huang W. A rapid method for detecting bacterial polyhydroxyalkanoates in intact cells by Fourier transform infrared spectroscopy. Appl Microbiol Biot 1999;51:523–6.
[27] Maquelin K, Kirschner C, Choo-Smith LP, van den Braak N, Endtz HP, Naumann D, et al. Identification of medically relevant microorganisms by vibrational spectroscopy. J Microbiol Meth 2002;51:255–71.
[28] Levine S, Stevenson HJR, Bordner RH. Identification of glycogen in whole bacterial cells by infrared spectrophotometry. Science 1953;118:141–2.
[29] Wong PTT, Lacelle S, Fung MFK, Senterman M, Mikhael NZ. Characterization of exfoliated cells and tissues from human endocervix and ectocervix by FTIR and ATR/FTIR spectroscopy. Biospectroscopy 1995;1:357–64.
[30] Ladygina N, Dedyukhina EG, Vainshtein MB. A review on microbial synthesis of hydrocarbons. Process Biochem 2006;41:1001–14.
[31] Warui DM, Li N, Norgaard H, Krebs C, Bollinger JM, Booker SJ. Detection of formate, rather than carbon monoxide, as the stoichiometric coproduct in conversion of fatty aldehydes to alkanes by a cyanobacterial aldehyde decarbonylase. J Am Chem Soc 2011;133:3316–9.
[32] Dembitsky VM, Dor I, Shkrob I, Aki M. Branched alkanes and other apolar compounds produced by the cyanobacterium *Microcoleus vaginatus* from the Negev Desert. Russ J Bioorg Chem 2001;27:110–9.
[33] Williams JGK. Construction of specific mutations in photosystem-ii photosynthetic reaction center by genetic-engineering methods in *Synechocystis* 6803. Method Enzymol 1988;167:766–78.
[34] Jones A, Davies HM, Voelker TA. Palmitoyl-acyl carrier protein (Acp) thioesterase and the evolutionary origin of plant acyl-acp thioesterases. Plant Cell 1995;7:359–71.
[35] Wada H, Murata N. Temperature-induced changes in the fatty-acid composition of the cyanobacterium, *Synechocystis* PCC6803. Plant Physiol 1990;92:1062–9.
[36] Luderitz O, Freudenberg MA, Galanos C, Lehman V, Rietschel ETH, shaw DH. Lipopolysaccharides of gram-negative bacteria. In: Razin S, Rottem S, editors. Membrane lipids of prokaryotes, vol. 17. New York, NY, USA: Academic Press, Inc.; 1982. p. 79–153.
[37] Lidstrom ME, Konopka MC. The role of physiological heterogeneity in microbial population behavior. Nat Chem Biol 2010;6:705–12.
[38] Walling MA, Shepard JRE. Cellular heterogeneity and live cell arrays. Chem Soc Rev 2011;40:4049–76.
[39] Wang DJ, Bodovitz S. Single cell analysis: the new frontier in 'omics'. Trends Biotechnol 2010;28:281–90.